

Octyl co-grafted PrSO₃H/SBA-15: tunable hydrophobic solid acid catalysts for acetic acid esterification

Jinesh C. Manayil,^[a] Vannia C. dos Santos,^[a] Friederike C. Jentoft,^[b] Marta Granollers Mesa,^[a] Adam F. Lee,^[a] and Karen Wilson*^[a]

Abstract: Propylsulfonic acid (PrSO₃H) derivatised solid acid catalysts have been prepared by post modification of mesoporous SBA-15 silica with mercaptopropyltrimethoxysilane (MPTMS), with the impact of co-derivatisation with octyltrimethoxysilane (OTMS) groups to impart hydrophobicity to the catalyst investigated. Turn over frequencies (TOF) for acetic acid esterification with methanol increase with PrSO₃H surface coverage across both families suggesting a cooperative effect of adjacent acid sites at high acid site densities. Esterification activity is further promoted upon co-functionalisation with hydrophobic octyl chains, with inverse gas chromatography (iGC) measurements indicating increased activity correlates with decreased surface polarity or increased hydrophobicity.

Introduction

The use of renewable resources for the sustainable production of transportation fuels and chemicals is currently of great interest due to growing concerns over the depletion of fossil fuel reserves and associated climate change.^[1] Thermochemical processing of lignocellulosic biomass through pyrolysis or gasification, and transesterification of non-edible and waste plant/algal oils and fats offers a promising solution to transform biomass for use in such applications.^[1-2] Fast pyrolysis of waste agricultural/forestry biomass for the production and subsequent upgrading of bio-oils to liquid transportation fuels has received considerable attention in this regard.^[3] However, the direct use of fast pyrolysis bio-oils is limited by its low heating value due to the high oxygen content, thermal instability, strong acidity and significant water content.^[4] Typical bio-oils are a mixture of acids, alcohols, furans, aldehydes, esters, ketones, sugars and multifunctional compounds such as hydroxyacetic acid, hydroxyacetaldehyde and hydroxyacetone (derived from cellulose and hemicellulose), together with 3-hydroxy-3-methoxybenzaldehyde, phenols, guaiacols and syringols derived from the lignin component.^[5] The production of transportation fuels from biomass-derived pyrolysis oils is therefore only viable if the oil is subjected to upgrading treatments including

ketonisation or esterification to reduce acidity prior to the final hydro-deoxygenation treatment.^[3b, 6]

Esterification of acetic acid, which is present in bio-oil at around 1-10 %, ^[4b] is an energy efficient and atom-economical means to improve bio-oil quality and stabilise the oil for further upgrading.^[3a] Suitable alcohols employed in esterification are either native to the bio-oil such as phenolics (guaiacol or cresol)^[3a] or externally sourced bio-derived alcohols such as methanol, ethanol and butanol. The use of homogenous mineral acids to catalyse esterification, while effective, requires subsequent quenching and neutralisation of the treated bio-oils, which results in large quantities of caustic waste streams and associated handling problems. Solid acid catalysts are thus sought to circumvent these problems by allowing facile separation and opportunities for continuous operation.

Typical solid acids explored for acetic acid esterification include sulfated zirconia, zeolites, heteropoly acids, and functionalised mesoporous silicas.^[3a, 6d, 7] Given the high water content of bio-oils is it also critical that solid acids are developed that exhibit excellent water tolerance or hydrophobicity. In this respect, mesoporous sulfonic acid silicas are a particularly interesting class of Brønsted acid catalyst^[8] that are widely explored in the context of biofuel related catalysis^[9] owing to their ability to allow both support architecture and surface polarity to be tuned. While these materials have received some attention for the esterification of acetic acid with methanol and benzyl alcohol^[10] in model bio-oils, the efforts to address the impact of hydrophobicity on esterification activity are limited. PrSO₃H/SBA-15 modified with propyl groups to impart hydrophobicity has been shown to exhibit increased water tolerance during acetic acid esterification when compared to H₂SO₄ or the conventional PrSO₃H/SBA-15 catalyst.^[10a] While this is a promising approach to tailoring catalysts for esterification reactions, our understanding of the interplay between surface polarity and activity is limited, hindering our ability to design improved catalyst formulations.

Inverse gas chromatography (iGC) is a powerful technique to probe the surface apolar and polar interactions of materials at a molecular level.^{[11] [12]} iGC measurements thus allow surface-adsorbate interactions to be investigated on porous catalysts, with thermodynamic properties including surface energy, hydrophobicity^[13] acid-base properties,^[14] heat of adsorption,^[15] and specific free energy^[16] to be determined. Evaluation of parameters such as surface polarity and hydrophobicity is critical for understanding how adsorption processes can be controlled in liquid and vapour phase catalysis. Here we report a study of a series of propyl sulfonic acid functionalised SBA-15 materials in which special attention has been paid to the effect of acid site density on the overall acidity and catalytic performance in acetic acid esterification with methanol. The effect of co-functionalising PrSO₃H/SBA-15 with octyltrimethoxysilane groups to impart hydrophobic character is subsequently investigated, with the

[a] Dr. Jinesh C. Manayil, Dr. Vannia C. dos Santos, Dr. Marta Granollers Mesa, Prof. Adam F. Lee, Prof. Karen Wilson. European Bioenergy Research Institute, Aston University, Birmingham, B4 7ET, UK
E-mail: k.wilson@aston.ac.uk

[b] Prof F.C. Jentoft
Department of Chemical Engineering,
University of Massachusetts Amherst,
MA 01003, USA

Supporting information for this article is given via a link at the end of the document.

impact on surface properties analysed using IGC.^[13] Calculated thermodynamic parameters are correlated with esterification activity, which in turn correlates with decreased surface polarity or increased hydrophobicity.

Results and Discussion

The successful synthesis of the parent SBA-15, and retention of the hexagonal close packed $p6mm$ pore architecture upon functionalisation with propyl sulfonic and octyltrimethoxysilane groups, was first assessed by low angle XRD and nitrogen adsorption isotherms (**Figs. S1** and **S2**).^[10c, 17] All functionalised materials show similar XRD patterns with common reflections at 1.07°, 1.75°, and 2.01° consistent with the parent SBA-15, confirmed that grafting, co-grafting and subsequent oxidation does not alter the pore order. The type IV isotherm with H1 hysteresis loop of SBA-15 is also maintained after derivatisation evidencing retention of mesoporosity.

The textural properties of PrSO₃H/SBA-15 and Oc/PrSO₃H/SBA-15 materials are summarised in **Table 1**. The BET surface area decreases slightly upon derivatisation with PrSO₃H groups, which is largely attributed to the loss of micropore area in the pore walls as determined from t-plot analysis, suggesting partial micropore blockage occurs during grafting. A slight decrease in the BJH mesopore diameter is also observed following sulfonic acid derivatisation, but the diameter remains in the range 4.6-4.8 nm for all functionalised samples. It is interesting to note that the micropore area associated with these intra-wall pores decreases steadily as a function of sulfonic acid loading, suggesting progressive filling of the micropores. The micropore surface area of the octyl co-derivatised samples decreases for all but the highest loaded PrSO₃H/SBA-15 sample, suggesting OTMS caps any unfunctionalised sites remaining in the micropore channels of the lower loaded PrSO₃H/SBA-15 samples.

The co-existence of sulfonic acid and octyl chains on the SBA-15 surface is confirmed by DRIFTS (**Fig. S3**). The parent SBA-15 shows characteristic bands at 700-1400 cm⁻¹ and 3000-3800 cm⁻¹ indicative of framework Si-O-Si and surface silanols

respectively.^[18] Following incorporation of sulfonic acid groups new weak bands centred ~2950 and 2854 cm⁻¹ evolve corresponding to CH₂ vibrations from alkyl chains.^{[19] [10c]} which increase in intensity with sulfonic acid loading. Further increases are observed, along with the emergence of a new peak at 2938 cm⁻¹ upon co-grafting with octyl chains as a result of the larger number of -CH₂ groups. Symmetric $\nu_{\text{sym}}(\text{CH})$ of methyl and methylene groups typically overlap, but the asymmetric stretches do not, this new band at 2938 cm⁻¹ is thus ascribed to $\nu_{\text{as}}(\text{CH}_2)$ of the methylene stretch.

CHNS analysis on both the parent PrSO₃H/SBA-15 and octyl co-functionalised samples show a steady increase in S content with the volume of MPTMS added during grafting process (**Table 1**). **Fig. 1** shows that the C:SO₃H molar ratio for the Oc/PrSO₃H/SBA-15 series decreases with increasing S content, thereby demonstrating the successful synthesis of a family of materials with tuneable surface acid site loading and loading of inert organic groups to tune hydrophobicity. **Fig. 1 (inset)** and **Table 1** show the acid site loading increases with S content for both PrSO₃H/SBA-15 and Oc/PrSO₃H/SBA-15 series. The surface acid site loading of the Oc/PrSO₃H-SBA-15 family was lower than the parent PrSO₃H/SBA-15 owing to a combination of the extra mass from octyl groups, and slight loss of thiol groups during the second grafting step. DRIFTS studies of pyridine adsorption confirm the presence of Brønsted acidic sites^[20] with bands at 1489, 1545 and 1637 cm⁻¹ indicative of pyridinium ion formation (**Fig. S4**).

NH₃ calorimetry (**Fig. S5**) revealed the acidic strength of PrSO₃H/SBA-15 to be invariant of sulfonic acid loading, with $\Delta H_{\text{ads}}(\text{NH}_3)$ determined to be -140 kJmol⁻¹. This was further corroborated by using Gutmann theory of acid-base interactions (**Equation 1**) which explains how the enthalpy of adsorption (ΔH_{SP}) of a probe molecule depends on the acceptor and donor number (A_N and D_N respectively) of the adsorbate and the acid and base constants of solid surface, (K_a and K_b respectively).

$$\Delta H_{\text{SP}} = A_N \cdot K_b + D_N \cdot K_a \quad (1)$$

Table 1 Textural and structural properties of PrSO₃H and Oc/PrSO₃H functionalised SBA-15 materials.

Materials	Surface area ^a /m ² g ⁻¹	BJH pore diameter / nm	Total BJH pore volume / cm ³ g ⁻¹	Unit cell parameter ^b /nm	Wall thickness ^c /nm	Micropore area /m ² g ⁻¹	Bulk S content ^d /wt.%	Bulk C content ^d / wt%	Acid site loading /mmol.g ⁻¹
SBA-15	759	4.9	0.76	10.17	5.24	305	-	0.80	-
0.15PrSO ₃ H/SBA-15	682	4.6	0.71	10.25	5.70	250	0.15	1.03	0.17
0.24PrSO ₃ H/SBA-15	637	4.6	0.68	10.19	5.64	228	0.24	1.39	0.21
0.42PrSO ₃ H/SBA-15	620	4.6	0.65	10.15	5.60	225	0.42	1.58	0.33
0.77PrSO ₃ H/SBA-15	663	4.7	0.77	10.19	5.52	115	0.77	1.80	0.44
Oc/0.15PrSO ₃ H/SBA-15	539	4.6	0.64	10.13	5.57	123	0.17	1.60	0.11
Oc/0.24PrSO ₃ H/SBA-15	545	4.6	0.61	10.15	5.58	127	0.23	1.88	0.12
Oc/0.42PrSO ₃ H/SBA-15	616	4.7	0.75	10.19	5.51	149	0.41	2.03	0.16
Oc/0.77PrSO ₃ H/SBA-15	587	4.8	0.64	10.09	5.30	148	0.69	2.35	0.28

^aBET. ^bDetermined from $a_0 = (2d100)/\sqrt{3}$. ^cDetermined from a_0 - pore diameter. ^dBulk S and C content from CHNS.

Calculation of acid constants from IGC measurements of the adsorption of methanol, acetonitrile, ethyl acetate and dichloromethane revealed similar values of K_a for low and high loading $\text{PrSO}_3\text{H/SBA-15}$ samples (**Fig. S5**).

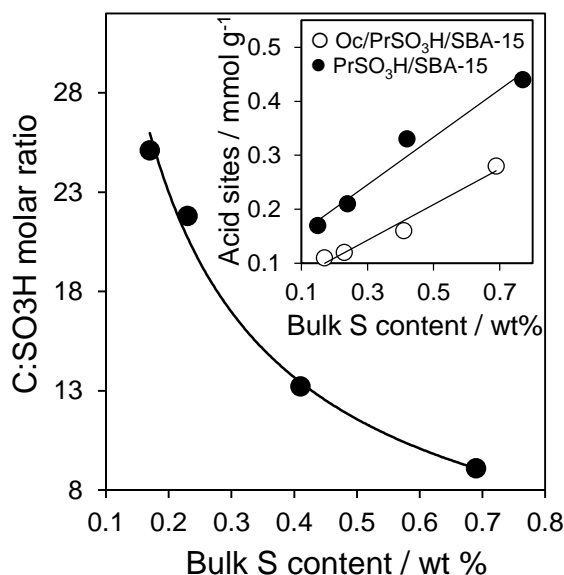
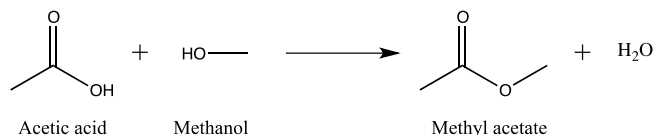


Figure 1. Bulk C:SO₃H molar ratio for Oc/PrSO₃H/SBA-15 catalysts as a function of S content. (inset) shows the evolution of acid site loading of Oc/PrSO₃H/SBA- and PrSO₃H/SBA as a function of bulk S content.

The influence of sulfonic acid group density and incorporation of hydrophobic octyl groups on esterification activity of the PrSO₃H/SBA-15 and Oc/PrSO₃H-SBA-15 materials was subsequently evaluated in acetic acid esterification with methanol (**Scheme 1**).



Scheme 1 Acetic acid esterification with methanol

Reaction profiles (**Fig. S6**) confirm that all sulfonic acid functionalised mesoporous silicas are active for esterification with the conversion increasing with PrSO₃H loading. Samples co-grafted with PrSO₃H and octyl groups exhibit comparable conversions to the parent PrSO₃H/SBA-15 (**Fig. S6**), with the highest loaded (Oc)PrSO₃H/SBA-15 catalysts achieving ~73% acetic acid conversion after 6h with 100% methyl acetate selectivity. In comparison, blank reactions in the absence of catalyst exhibited < 8 % acetic acid conversion after 6 h (**Fig. S7**). For both families of catalyst, initial rates of acetic acid conversion increase with acid site density (**Fig S8**), reflecting the direct impact of increased Brönsted acidity on activity. Turnover Frequencies (TOFs) for the PrSO₃H/SBA-15 series (**Fig. 2**) were found to increase as a function of surface acid site density, reaching a plateau for coverages > 0.3 H⁺.nm⁻². Octyl post functionalisation results in a further enhancement of the TOFs,

suggesting the hydrophobic character imparted by the octyl chain assists with inhibiting reverse ester hydrolysis as previously reported for PrSO₃H/MCM41.^[19] This change in TOF observed for both families with PrSO₃H loading could be attributed to more densely packed PrSO₃H groups favouring cooperative interactions, as previously suggested for sol-gel prepared PrSO₃H/SBA-15^[10b] and grafted PrSO₃H/MCM-41.^[19] High sulfonic acid site densities are also reported to favour a Langmuir-Hinshelwood (LH) mechanism for acetic acid esterification.^[10b] Kinetic modelling determined activation energies of 42.6 kJmol⁻¹ for the LH mechanism, which was slightly lower than the 45.6 kJmol⁻¹ determined for an Eley Rideal (ER) pathway. SAC-13 sulfonic acid resin catalysts, which follow an ER mechanism for acetic acid esterification,^[21] are also associated with high activation energies of 63.8 kJmol⁻¹. Apparent activation energies could thus be used to reflect whether there is a change in cooperativity across series of grafted PrSO₃H/SBA-15 catalysts. Activation energies for acetic esterification for the lowest (0.15-PrSO₃H/SBA-15) and highest loaded (0.77-PrSO₃H/SBA-15) materials were determined to be 63±5 kJmol⁻¹ and 51±5 kJmol⁻¹ respectively (**Fig S9**) in accord with the hypothesis that a change in mechanism may be induced with PrSO₃H density: isolated PrSO₃H groups favour an ER pathway, while decreased acid site separation upon increasing active site loading and PrSO₃H density favours LH pathways. It is interesting to note that literature values, which were measured in a 1,4-dioxane solvent^[10b] are slightly lower than the values determined here. This may reflect the impact of solvent effects influencing the reaction kinetics due to both reactant and product solubility and competitive adsorption for surface acid sites.

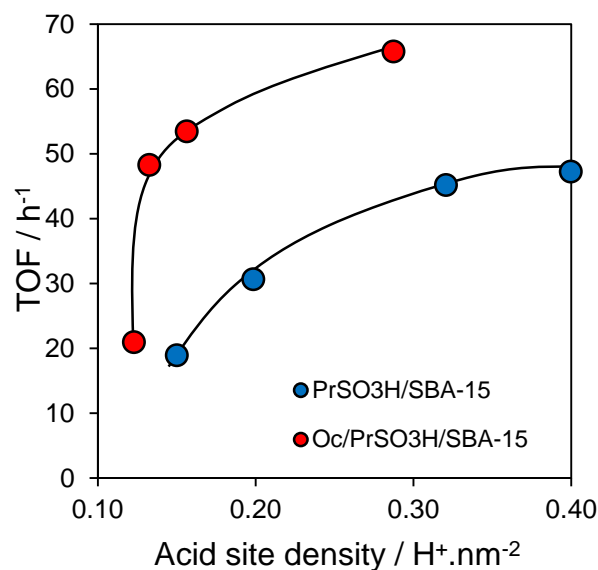


Fig. 2 Effect of acid site density on TOF for acetic acid esterification over PrSO₃H/SBA-15 and Oc/PrSO₃H/SBA-15 catalysts. Reaction conditions: 50 mg catalyst, 60 °C, acid:alcohol ratio of 1:30

To verify the effect of octyl chains in improving water tolerance, the esterification activity of 0.77-PrSO₃H/SBA-15 and Oc/0.77-PrSO₃H/SBA-15 was compared following addition of 1 and 10 mmol of water (**Fig. S10**). The Oc/PrSO₃H/SBA-15 catalyst exhibited a negligible change in TOF upon addition of 1 mmol water (1:5 molar ratio of water:acid), which was in contrast to the

parent PrSO₃H/SBA-15 sample whose TOF decreases by 20% (Fig 3). The apparent water tolerance under these conditions surpasses previous studies of propyl co-functionalised PrSO₃H/SBA-15 where initial rates decrease by 35% upon addition of similar levels of water (1:6 molar ratio water:acid).^[10a] The beneficial effect of co-grafting with hydrophobic octyl chains was particularly evident upon addition of 10 mmol water (significantly in excess of normal reaction conditions), where despite the expected decrease in activity under such challenging conditions, the TOF for Oc/PrSO₃H/SBA-15 was still 43% higher than the parent PrSO₃H/SBA-15.

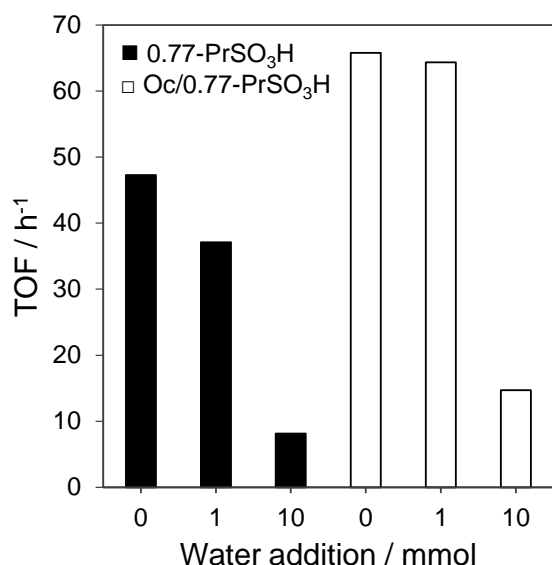


Fig. 3 Impact of water addition on acetic acid esterification with methanol over 0.77-PrSO₃H/SBA-15 and Oc/0.77-PrSO₃H/SBA-15.

To further check the influence of octyl chains in driving reactively formed water away from the acid site, the activity of 0.77PrSO₃H/SBA-15 and Oc/0.77PrSO₃H/SBA-15 catalysts was subsequently evaluated under a stoichiometric acetic acid to MeOH molar ratio. While the equilibrium acetate yield will be reduced under such conditions, the kinetics should be more sensitive towards accumulation of reactively formed water on the catalyst than observed at higher alcohol concentrations. Thus, the hydrophobic Oc/0.77PrSO₃H/SBA-15 material should exhibit sustained activity due to removal of reactively formed water, whereas the hydrophilic 0.77PrSO₃H/SBA-15 catalyst will be expected to deactivate. This is indeed what is observed as shown in Fig. S11 which demonstrates the hydrophobic octyl co-functionalised Oc/0.77PrSO₃H/SBA-15 catalyst exhibits over twice the activity of the more hydrophilic counterpart 0.77PrSO₃H/SBA-15, confirming the impact of octyl chains in inhibiting the reverse ester hydrolysis.

The stability of the Oc/0.77PrSO₃H/SBA-15 and 0.77PrSO₃H/SBA-15 catalysts was further evaluated by recycle and hot filtration tests. Fig S12 demonstrates that excellent recyclability was observed, with only a small decrease in conversion and TOF observed on reuse. Further leaching studies conducted via hot filtration tests (Fig. S13) reveal there

is negligible conversion upon removal of both sulfonic and octyl co-functionalised catalysts from reaction after 1h reaction.

The improved water tolerance of Oc/PrSO₃H/SBA-15 catalysts is significant for the development of catalysts for esterification reactions. However, despite such effects often being claimed to relate to increased hydrophobicity there remains a dearth of analytical studies that quantify such properties of catalyst materials. The hydrophobicity of a surface can originate from a change in surface polarity, which can be determined from surface energy calculations. Recently we have reported on the application of inverse gas chromatography (IGC) as a means of quantifying the specific and non-specific interactions of polar and non-polar hydrocarbon adsorbates on periodic mesoporous organo-silicas,^[13] which can be related to hydrophobicity. Building upon this work, IGC has been applied to elucidate the surface energy and surface adsorption properties of the current family of octyl co-grafted sulfonic acid silicas. IGC can deliver the physical (dispersive) and chemical (specific/polar/acid-base) surface energy associated with the materials from adsorption measurements of alkane and acid-base probe molecules respectively. Non-polar molecules adsorb via non-specific London forces while polar molecules interact through acid-base, hydrogen bonding interactions.^[15, 22] The total surface energy is thus the sum of the dispersive and specific component from all interactions,^[23] with the dispersive component calculated as per Equation 2, from the slope of the plot between RTlnV_N vs a(γ_L^D)^{1/2} (Fig. S14).^[13]

$$RT\ln V_N = 2N_A(\gamma_S^D)^{1/2} a(\gamma_L^D)^{1/2} + \text{constant} \quad (2)$$

In this instance N_A is Avagadro's number, a is the surface area of the probe molecule, V_N is the specific retention volume of the adsorbate, and γ_S^D and γ_L^D are dispersive components of the solid and liquid surface energy respectively.

The standard free energy of adsorption can also be calculated from the sum of dispersive and specific free energies (Equations 3 and 4).

$$\Delta G_{ads} = \Delta G_{ads}^D + \Delta G_{ads}^{SP} \quad (3)$$

$$\Delta G_{ads} = -RT\ln V_N + \text{constant} \quad (4)$$

The specific free energy due to polar interactions can be calculated from the deviation of calculated RTlnV_N values from the gradient of the plot of RTlnV_N v's a(γ_L^D)^{1/2} obtained from dispersion forces from non-polar adsorbates (Fig. S14).^[13, 22c]

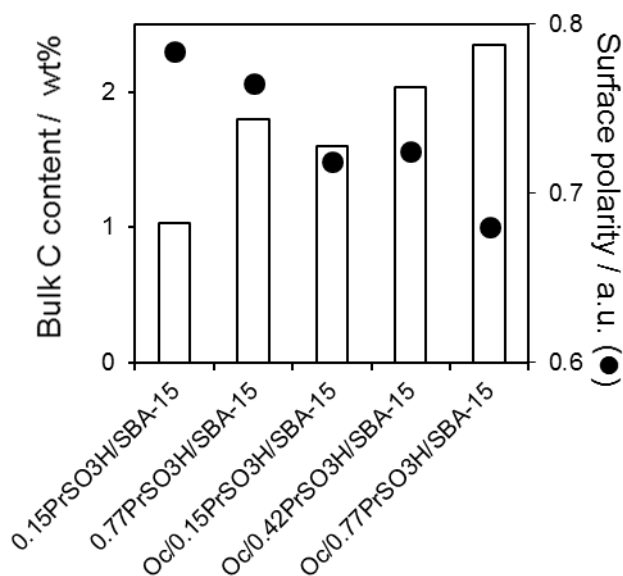
Measurement of adsorption isotherms under conditions of infinite dilution (in the Henry region - when the isotherm is linear and only interactions of the probe molecule with the material surface exist^[15]) also allows the differential isosteric heat of adsorption to also be calculated (Fig S15) from temperature dependent plots of volume (V_{ads}) adsorbed vs p/p₀. Surface polarity, X_p is calculated as the ratio of the polar surface energy to the total surface energy^[23] (Equation 5) using values from Table 2 and Fig. S14.

$$X_p = \gamma_S^{SP} / (\gamma_S^{SP} + \gamma_S^D) \quad (5)$$

Fig 4 shows that the surface polarity for both Oc/PrSO₃H/SBA-15 and PrSO₃H/SBA-15 samples decreases with increased carbon content, suggesting surface polarity is a useful parameter to reflect the change in surface properties.

Table 2 Evolution of surface properties of PrSO₃H/SBA-15 and Oc/PrSO₃H/SBA-15 with low and high S content

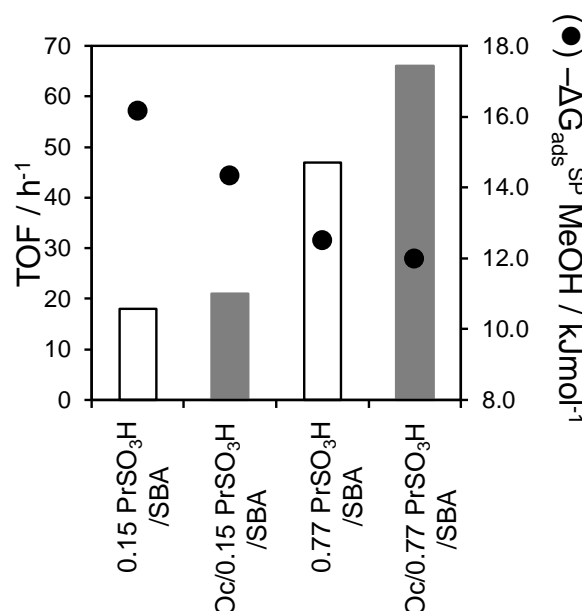
Materials	IGC results			
	Disp. Surf. Energy (γ_s^D) / mJ m ⁻²	Sp. Surf. Energy (γ_s^{SP}) / mJ m ⁻²	$-\Delta G_{ads}^{SP}$ methanol / kJ mol ⁻¹	$-\Delta H$ methanol / kJ mol ⁻¹
0.15PrSO ₃ H/SBA-15	74	269	16	74
Oc/0.15PrSO ₃ H/SBA-15	50	130	13	61
0.77PrSO ₃ H/SBA-15	65	211	14	75
Oc/0.77PrSO ₃ H/SBA-15	42	89	12	64

**Fig. 4** Correlation between bulk carbon content from octyl group incorporation and the surface polarity of PrSO₃H/SBA-15 and Oc/PrSO₃H/SBA-15 catalysts.

$\Delta H_{ads}(\text{methanol})$ over sol-gel PrSO₃H/SBA-15,^[10b] is reported to be similar to that for water, suggesting methanol and water binding characteristics will respond similarly and the former can be used to assess hydrophobicity. **Table 2** shows that for methanol adsorption both $-\Delta G_{ads}^{SP}$ and $-\Delta H_{ads}$ decrease upon octyl co-functionalisation, indicating methanol binding is weaker than over the parent PrSO₃H/SBA-15. Methanol adsorption isotherms also reveal that methanol surface coverage is reduced over octyl co-functionalised samples, further supporting the weakened surface interactions with polar molecule (**Fig. S16**).

Fig. 5 shows that the increased TOFs for acetic acid esterification over PrSO₃H/SBA-15 and OcPrSO₃H/SBA-15 can be correlated with a decrease in $-\Delta G_{ads}^{SP}$ for methanol adsorption. The impact of tuning bulk carbon content on associated surface polarity and TOF for esterification is correlated in **Fig. 6**, which reveals decreased surface polarity (inversely related to surface hydrophobicity) leads to an increased TOF. Thus, it can be deduced the promotional effect of octyl groups on esterification activity can be predicted from changes in surface polarity. Decreased surface polarity, or increased hydrophobicity serves to both to displace the water by-product while also weakening the interaction with methanol.

The latter point may be particularly important in enhancing acetic acid adsorption during an LH mechanism when methanol is in vast excess. Given the calculated adsorption energy of acetic acid on PrSO₃H is approximately -140 kJ/mol,^[10b] (higher than both methanol and ethanol) excess alcohol will be required to favour adsorption and open up the LH pathway.

**Fig. 5** Correlation between $-\Delta G_{ads}^{SP}$ for methanol adsorption and TOF for acetic acid esterification with methanol over PrSO₃H/SBA-15 and Oc/PrSO₃H/SBA-15 catalysts.

The activity of PrSO₃H/SBA-15 and OcPrSO₃H/SBA-15 with high sulfonic acid loadings is in good agreement with our previous studies of octyl co-grafted of PrSO₃H/MCM-41,^[19] and reports on the effect of PrSO₃H loading on SBA-15 (achieved by partial poisoning of acid sites with pyridine)^[10a] where a two site cooperative mechanism for esterification is proposed. Increased surface PrSO₃H density brings acid head groups in closer proximity increasing the probability of a two-centre reaction between acetic acid and methanol adsorbed on adjacent PrSO₃H sites. However, Molecular Dynamic simulations on PrSO₃H/MCM-41 demonstrated that at low acid site loadings, flexing of PrSO₃H chains led to hydrogen bonding interaction with free surface silanol groups, which decreased acid strength.

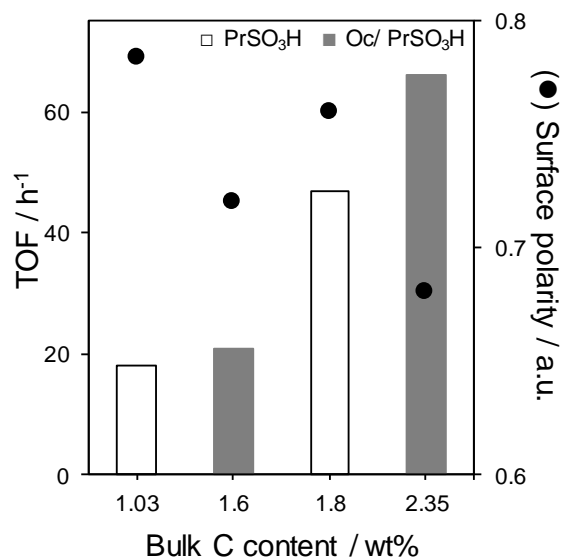
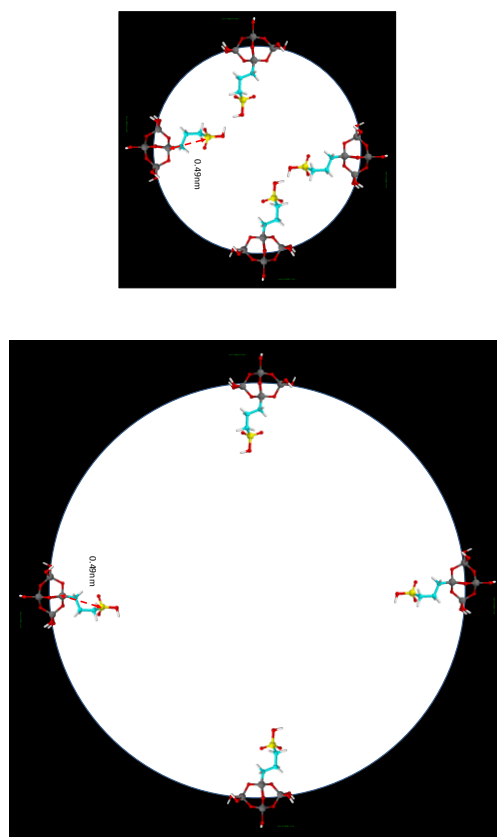


Fig. 6 Dependence of acetic acid esterification and surface polarity over functionalised SBA-15 on alcohol. Reaction conditions: 50 mg catalyst, 60 °C, acid:alcohol ratio of 1:30.

Capping of free silanol groups with OTMS, in addition to increasing hydrophobicity, lifted this interaction thereby increasing acid strength and favouring increased cooperativity between sulfonic acid head groups. On SBA-15 however, the observation that acid strength is invariant of PrSO₃H loading suggests there is a subtle difference in the surface interactions of sulfonic acid groups at low loadings over the two supports, which could be accounted for by a difference in surface hydroxyl distributions or pore diameter for the two classes of material.

Scheme 2 shows a scaled illustration of sulfonic acid groups grafted within 2.5 and 4.5 nm pores characteristic of MCM-41 and SBA-15 respectively. The high curvature of the smaller mesopores of MCM-41 (**Scheme 2a**), will result in (i) PrSO₃H head-groups coming into contact with the pore wall more readily upon flexing of the alkyl chain, and (ii) PrSO₃H situated around the pore to interact with each other more readily via cross pore interactions as suggested previously for organically modified silicas.^[24] In contrast for the larger, low curvature pores of SBA-15 (**Scheme 2b**) steric restrictions in the propyl chain flexing means SO₃H head groups cannot readily hydrogen bond to the surface, thus acid strength will not be impaired at low loading via such interactions.

Assuming a uniform distribution of sulfonic acid groups, this also indicates that on geometric grounds, small mesopores should exhibit a higher probability for cooperative interactions at low fractional surface coverages of PrSO₃H groups. Larger pore materials should require higher loadings, or grafting to occur in islands to facilitate cooperative interactions. This hypothesis raises some interesting questions about the effect of pore confinement of functional groups in sulfonic acid silicas, and the tendency for them to promote LH or ER kinetic mechanisms. Further studies by molecular dynamic simulations and kinetic modelling are required to address these questions.



Scheme 2 Illustration of how cooperative effects between sulfonic acid groups could occur (top) across the pore in 2.5 nm pores characteristic of MCM-41, whereas in (bottom) such interactions are less favoured for 4.5 nm pores representing SBA-15. Larger pores would require higher loadings, or grafting to occur in islands to facilitate cooperative interactions.

Conclusions

A series of propyl sulfonic acid and octyl co-functionalised propyl sulfonic acid SBA-15 silicas have been evaluated for potential application in bio-oil pre-treatments using acetic acid esterification with methanol as a model system. The turn over frequency for acetic acid esterification with methanol is enhanced upon both increasing surface sulfonic acid site density, and hydrophobicity by introduction of octyl groups. Octyl cofunctionalised catalysts also showed excellent water tolerance suggesting their suitability for use in esterification pretreatments of pyrolysis bio-oils. Increased surface acid site density is believed to induce cooperative interactions between acid sites which directs esterification via a LH mechanism. More isolated sites present at low sulfonic acid loadings exhibit higher activation barriers for reaction and are proposed to favour an ER pathway. The evolution of surface properties with functional group loading was followed using inverse gas chromatography (IGC) which corroborates that octyl group incorporation decreases surface polarity and increases surface hydrophobicity. IGC measurements also indicate that in addition to increasing the surface hydrophobicity, capping of free surface hydroxyl groups decreases the free energy of methanol adsorption. The

surface adsorption characteristics determined via IGC correlate well with catalytic performance, suggesting this is a powerful tool to study the effect of hydrophobicity in catalysis.

Experimental Section

Catalyst synthesis

SBA-15 was synthesised adopting the protocol of Zhao and co-workers.[17a] Typically 10 g of Pluronic P123 triblock copolymer was dissolved in 75 ml of water and 250 ml of 2M HCl solution. The mixtures were stirred at 35 °C for dissolution and then 23 ml of TEOS was added with the synthesis maintained at 35 °C for 20 h under stirring. The resulting gel was then aged at 80 °C for 24 h. Finally, the solid product was filtered, washed with water and calcined under static air at 550 °C for 5 h.

A series of sulfonic acid functionalised SBA-15 and its octyl co-derivatized forms were prepared following reported method.[10c, 19] MPTMS in toluene was initially prepared as precursor for grafting on SBA-15. Specific amount of MPTMS in toluene ($0.01 < \text{MPTMS/SBA-15} < 1$) was added per gram of material to vary the thiol coverage from low to high on SBA-15. The mixture then refluxed for 24 hours in 30 ml of toluene. Thiol functionalised samples were then filtered washed with methanol and dried at 80 °C. One portion of thiol functionalised samples was oxidised with H₂O₂ at room temperature for 24 h (30 ml of 33 wt% H₂O₂ per gram of material) to prepare sulfonic functionalised SBA-15 and the other portion used for co-grafting with octyl groups. The series is represented as (x)PrSO₃H/SBA-15 where x gives the wt% S measured by CHNS.

The octyl grafted materials are synthesised from the un-oxidised thiol grafted SBA-15 series. The un-oxidised thiol grafted samples (~1g) from the above batch was refluxed in 30 ml of toluene for 24h with 1 ml of octyltriethoxysilane.[19] The octyl co-grafted samples are then filtered, washed with methanol, dried and oxidised with H₂O₂ at room temperature for 24 h (30 ml of 33 wt% H₂O₂ per gram of material) to convert thiol groups to sulfonic acid. S and C contents of the final octyl co-derivatised samples were remeasured by CHNS analysis. For simplicity, this series is denoted as Oc/(x)PrSO₃H/SBA-15 where x gives the wt% S measured by CHNS in the parent sample.

Characterisation

Physicochemical properties of the as-synthesised catalysts were fully characterised. Low angle XRD patterns were recorded on a Bruker D8 Advance diffractometer fitted with an X'celerator detector and Cu K_α (1.54 Å) source over the range $2\theta = 0.3\text{-}10^\circ$. Nitrogen porosimetry was measured on a Quantachrome Nova 4000 porosimeter and analysed with NovaWin software. Samples were degassed at 120 °C for 4 h prior to analysis at -196 °C. Bulk sulphur loadings were calculated using XRF analysis on a Bruker S8 Tiger and verified by CHNS analysis using Thermo Scientific Flash 2000 CHNS-O analyser. DRIFTS measurements were conducted using a Thermo Scientific Nicolet environmental cell and smart collector accessory on a Thermo Scientific Nicolet iS50 FT-IR Spectrometer with MCT detector. The catalysts diluted in KBr (10 wt%) were loaded in the environmental cell and subjected to evacuation at 200 °C for 2 h to remove physisorbed water/moisture. Analyses were performed at 200 °C. Ex-situ pyridine adsorption studies were made by wetting the samples with pyridine. Excess pyridine was removed overnight in vacuo at 50 °C, with subsequent in vacuo analysis by

DRIFTS at 50 °C. Acid sites concentrations were measured by NH₃ pulse chemisorption using a Quantachrome ChemBET 3000 instrument interfaced to an MKS Minilab mass spectrometer (MS). Samples were degassed at 120 °C overnight under helium prior to NH₃ pulse titration at 100 °C. Temperature-programmed desorption (TPD) was subsequently performed on ammonia saturated samples between 100-500 °C. Ammonia adsorption calorimetry under flow conditions was performed using a system based on a flow-through Setaram111 differential scanning calorimeter (DSC) and an automated gas flow and switching system, with down-stream mass spectrometer detector (Hiden HPR20) connected via a heated capillary. In a typical experiment, the sample (5–15 mg) was activated under dried helium (5 ml min⁻¹) for 2 h at 100 °C. Adsorption was monitored at 100°C, so measured enthalpies correspond only to ammonia that binds irreversibly to the catalyst at this temperature. Small pulses (typically 1 mL) of the probe gas (1% ammonia in helium) were then injected at regular intervals into the carrier gas stream from a gas sampling valve, also at 100 °C. The concentration of ammonia downstream of the sample was monitored with the mass spectrometer ($m/z=15$), and heat evolution with the calorimeter. The net amount of ammonia irreversibly adsorbed from each pulse was determined by comparing the mass spectrometer signal during each pulse with a signal recorded through a blank sample tube during a control experiment. Net heat released for each pulse was calculated from the DSC thermal curve. From this the molar enthalpy of ammonia adsorption ΔH° Ads NH₃ was obtained for the ammonia adsorbed from each pulse.

Inverse gas chromatography

IGC at infinite dilution was used to explore surface energies, heat of sorption, adsorption isotherms and associated structure-activity relationships^[13-16]. All the measurements were performed at infinite dilution in the Henry region ($p/p_0 = 0.04$) to exclude interactions between probe molecules on material surface. Measurements were performed using a Surface Measurement System IGC with IGC controller v1.8 software. The samples (~10 mg) are packed in a 3 mm diameter column and degassed at 120 °C for 2 hours prior to analysis. Detailed experimental procedure is given in the ESI. Surface energy measurements were carried out with apolar (hexane, heptane, octane, nonane, and decane) and polar (methanol, acetonitrile, ethyl acetate, and dichloromethane) probes to calculate both dispersive (γ_s^D) and specific (γ_s^{SP}) component of surface energy respectively.^[15] Heat of sorption studies were performed by injecting a specific amount of methanol in a temperature window of 90 to 100 °C. Adsorption isotherms were recorded by injecting alcohol over the range, $p/p_0 = 0.02$ to 0.1 at 80 °C.

Esterification

The reaction conditions for acetic acid esterification with methanol employed conditions that have previously been optimised by our group.^[19, 25] Briefly, esterification reactions were performed in batch at 60 °C employing 0.05 g of catalyst, 5 mmol of acetic acid, 150 mmol of alcohol (acid:alcohol mole ratio 1:30), and 0.5 mmol of dihexyl ether as an internal standard.^[18-19, 25] Aliquots were withdrawn periodically from the reaction mixture diluted with methanol and analysed by off-line GC using a Varian 450-GC equipped with a ZB 50 15 m × 0.25 mm × 0.25 μm capillary column. Reactions performed at a 1:1 methanol:acetic acid ratio were performed using 0.020 g catalyst with 20 mmol alcohol and acid so as to overcome mixing problems with small reaction volumes under solvent free conditions. Turnover Frequencies (TOFs) were calculated by normalising initial rates derived from the linear portion of reaction profiles during the first hour to the acid site loadings obtained from NH₃ pulse chemisorption. Water spiking experiments were performed with addition of 1 and 10 mmol of water. Hot filtration experiments were performed in which the catalyst was removed from the reaction after 1 hour by hot

filtration, with further conversion of the filtrate monitored for an additional 6 h.

Acknowledgements

We thank the EPSRC for financial support (EP/K000616/2, EP/G007594/4 and EP/K014749/1) and the award of a Leadership Fellowship to AFL. KW thanks the Royal Society for an Industry Fellowship. Support from the European Union Seventh Framework Programme (FP7/2007-2013) under grant agreement no. 604307 is also acknowledged. VCS acknowledges CNPq (Conselho Nacional de Desenvolvimento Científico e Tecnológico) for the award of a postdoctoral scholarship Text. FCJ acknowledges support though NSF Award 1560519.

Keywords: Sulfonic acid • bio-fuels • esterification • hydrophobicity • SBA-15

References:

- [1] G. W. Huber, S. Iborra, A. Corma, *Chemical Reviews* **2006**, *106*, 4044-4098.
- [2] aA. F. Lee, J. A. Bennett, J. C. Manayil, K. Wilson, *Chemical Society Reviews* **2014**, *43*, 7887-7916; bA. F. Lee, K. Wilson, *Catalysis Today* **2015**, *242*, 3-18.
- [3] aL. Ciddor, J. A. Bennett, J. A. Hunns, K. Wilson, A. F. Lee, *Journal of Chemical Technology and Biotechnology* **2015**, *90*, 780-795; bS. Zhang, Y. Yan, T. Li, Z. Ren, *Bioresource Technology* **2005**, *96*, 545-550.
- [4] aA. Alcalá, A. V. Bridgwater, A. Alcalá, A. V. Bridgwater, *blends of biodiesel and pyrolysis oil* **2014**, *109*, 417-426; bC. A. Mullen, A. A. Boateng, N. M. Goldberg, I. M. Lima, D. A. Laird, K. B. Hicks, *Biomass and Bioenergy* **2010**, *34*, 67-74; cD. Mohan, C. U. Pittman, P. H. Steele, *Energy & Fuels* **2006**, *20*, 848-889.
- [5] aQ. Zhang, J. Chang, T. Wang, Y. Xu, *Energy Conversion and Management* **2007**, *48*, 87-92; bC. A. Mullen, A. A. Boateng, *Energy & Fuels* **2008**, *22*, 2104-2109.
- [6] aP. M. Mortensen, J. D. Grunwaldt, P. A. Jensen, K. G. Knudsen, A. D. Jensen, *Applied Catalysis A: General* **2011**, *407*, 1-19; bA. V. Bridgwater, *Biomass and Bioenergy* **2012**, *38*, 68-94; cA. H. Zacher, M. V. Olarte, D. M. Santosa, D. C. Elliott, S. B. Jones, *Green Chemistry* **2014**, *16*, 491-515; dM. Milina, S. Mitchell, J. Pérez-Ramírez, *Catalysis Today* **2014**, *235*, 176-183.
- [7] aG. X. Yu, X. L. Zhou, C. L. Li, L. F. Chen, J. A. Wang, *Catalysis Today* **2009**, *148*, 169-173; bN. Lohitham, B. H. Shanks, *Catalysis Communications* **2009**, *11*, 96-99.
- [8] aK. Wilson, A. F. Lee, D. J. Macquarrie, J. H. Clark, *Applied Catalysis A: General* **2002**, *228*, 127-133; bJ. A. Melero, G. D. Stucky, R. van Grieken, G. Morales, *Journal of Materials Chemistry* **2002**, *12*, 1664-1670; cS. Shylesh, S. Sharma, S. P. Mirajkar, A. P. Singh, *Journal of Molecular Catalysis A: Chemical* **2004**, *212*, 219-228; dA. F. Lee, K. Wilson, in *Handbook of Green Chemistry*, Wiley-VCH Verlag GmbH & Co. KGaA **2010**; eC. Pirez, M. T. Reche, A. F. Lee, J. C. Manayil, V. C. dos-Santos, K. Wilson, *Catalysis Letters* **2015**, *145*, 1483-1490.
- [9] aC. Pirez, A. F. Lee, J. C. Manayil, C. M. A. Parlett, K. Wilson, *Green Chemistry* **2014**, *16*, 4506-4509; bJ. A. Melero, L. F. Bautista, G. Morales, J. Iglesias, R. Sánchez-Vázquez, *Chemical Engineering Journal* **2010**, *161*, 323-331.
- [10] aS. Miao, B. H. Shanks, *Applied Catalysis A: General* **2009**, *359*, 113-120; bS. Miao, B. H. Shanks, *Journal of Catalysis* **2011**, *279*, 136-143; cJ. C. Manayil, C. V. M. Inocencio, A. F. Lee, K. Wilson, *Green Chemistry* **2016**.
- [11] aL. Boudriche, R. Calvet, B. Hamdi, H. Balard, *Colloids and Surfaces A: Physicochemical and Engineering Aspects* **2011**, *392*, 45-54; bJ. A. F. Gamelas, J. Pedrosa, A. F. Lourenço, P. J. Ferreira, *Colloids and Surfaces A: Physicochemical and Engineering Aspects* **2015**, *469*, 36-41; cD. Gavril, *Catalysis Today* **2015**, *244*, 36-46.
- [12] J. M. R. C. A. Santos, J. T. Guthrie, *Journal of Chromatography A* **2015**, *1379*, 92-99.
- [13] C. Pirez, A. F. Lee, C. Jones, K. Wilson, *Catalysis Today* **2014**, *234*, 167-173.
- [14] T. Hamieh, M.-B. Fadlallah, J. Schultz, *Journal of Chromatography A* **2002**, *969*, 37-47.
- [15] M. Rückriem, D. Enke, T. Hahn, *Microporous and Mesoporous Materials* **2015**, *209*, 99-104.
- [16] L. Boudriche, R. Calvet, B. Hamdi, H. Balard, *Colloids and Surfaces A: Physicochemical and Engineering Aspects* **2012**, *399*, 1-10.
- [17] aD. Y. Zhao, J. L. Feng, Q. S. Huo, N. Melosh, G. H. Fredrickson, B. F. Chmelka, G. D. Stucky, *Science* **1998**, *279*, 548-552; bD. Y. Zhao, Q. S. Huo, J. L. Feng, B. F. Chmelka, G. D. Stucky, *Journal of the American Chemical Society* **1998**, *120*, 6024-6036.
- [18] C. Pirez, K. Wilson, A. F. Lee, *Green Chemistry* **2014**, *16*, 197-202.
- [19] J.-P. Dacquin, H. E. Cross, D. R. Brown, T. Duren, J. J. Williams, A. F. Lee, K. Wilson, *Green Chemistry* **2010**, *12*, 1383-1391.
- [20] L. M. Parker, D. M. Bibby, G. R. Burns, *Journal of the Chemical Society, Faraday Transactions* **1991**, *87*, 3319-3323.
- [21] Y. Liu, E. Lotero, J. G. Goodwin Jr, *Journal of Catalysis* **2006**, *242*, 278-286.
- [22] aF. M. Fowkes, *Industrial & Engineering Chemistry* **1964**, *56*, 40-52; bU. Panzer, H. P. Schreiber, *Macromolecules* **1992**, *25*, 3633-3637; cJ. B. Donnet, S. J. Park, H. Balard, *Chromatographia*, *31*, 434-440.
- [23] J. S. Kim, R. H. Friend, F. Cacialli, *Journal of Applied Physics* **1999**, *86*, 2774-2778.
- [24] N. A. Brunelli, C. W. Jones, *Journal of Catalysis* **2013**, *308*, 60-72.
- [25] C. Pirez, J.-M. Caderon, J.-P. Dacquin, A. F. Lee, K. Wilson, *ACS Catalysis* **2012**, *2*, 1607-1614.
